Supporting Information for

Probing deep into the interaction of a fluorescent chalcone derivative and bovine serum albumin (BSA): An experimental and computational study

Haline G. O. Alvim,[a,b] Emma L. Fagg,[a,b] Aline. L. Oliveira,[a,b] Heibbe C. B. de Oliveira,[a,b] Sonia M. Freitas,[c] Mary-Ann E. Xavier,[c] Thereza A. Soares,[d] Alexandre F. Gomes,[e] Fabio C. Gozzo,[e] Wender A. Silva,[*b] and Brenno A. D. Neto,[*a]

[a] *Laboratory of Medicinal and Technological Chemistry, University of Brasilia (IQ-UnB). Campus Universitário Darcy Ribeiro, CEP 70904970, P.O.Box 4478, Brasilia-DF, Brazil; E-mail: brenno.ipi@gmail.com*

[b] *Laboratory for Bioactive Compounds Synthesis, University of Brasilia (IQ-UnB). Campus Universitário Darcy Ribeiro, CEP 70904970, P.O.Box 4478, Brasilia-DF, Brazil; E-mail: wender@unb.br*

[c] *Laboratório de Biofísica, Depto de Biologia Celular (IB-UnB), Universidade de Brasília, UnB. Brasília, DF, Brazil.*

[d] *Departamento de Quı´mica Fundamental, UFPE, Av. Jornalista Anibal Fernandes, s/n - Cidade Universitaria, 50740-560, Recife-PE, Brazil.*

[e] *Institute of Chemistry, University of Campinas, Campinas, SP, Brazil.*

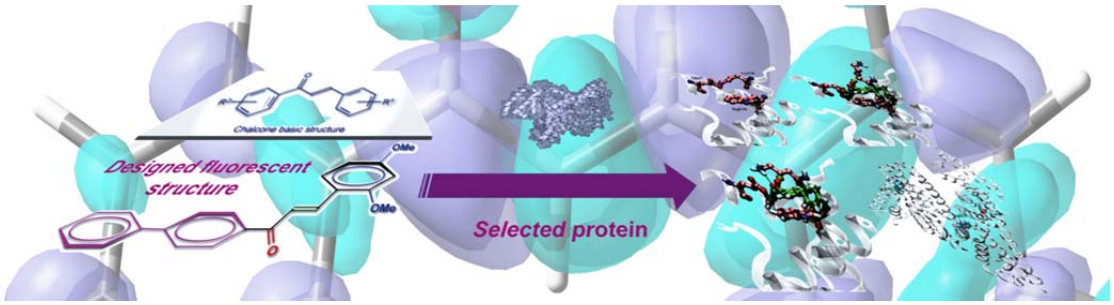

Materials and methods

Chemicals and solvents were purchased from commercial sources and used without further purification.

Synthesis of fluorescent chalcone 3

Chalcone derivative **3** was obtained from a classic aldol condensation (Claisen-Schmidt condensation) of aromatic aldehydes and aromatic ketones in excellent yield (90%) after purification. Ketone **1** (1 mmol) was added to a solution of NaOH (10% *w/v* or KOH) and ethanol (3 mL). The mixture was stirred for 20 min under ice bath cooling. After, aldehyde **2** (1 mmol) was added and the resulting mixture was stirred for additional 12 hours at room temperature. The reaction mixture was acidified with HCl 10%. The precipitate was collected, washed with cold water, dried and purified by column chromatography (20% ethyl acetate/hexane). See Table 3 in the main text to access spectroscopic data for **3**. *Anal. Calcd* for $C_{23}H_{20}O_3$: C, 80.21; H, 5.85; N, 0.00. Found: C, 80.39; H, 5.97; N, 0.00. m.p. 84-85 °C.

NMR measurements

All NMR measurements were carried out on a Bruker Avance III spectrometer (11.75 T) operating at 500 MHz for ^{1}H and on a Varian Mercury Plus spectrometer (7.05 T) operating at 300 MHz for ^{1}H and at 75.46 MHz for ^{13}C.

NMR samples were prepared by dissolving 40 mg of chalcone **3** in 600 μL of DMSO-*d6* containing TMS as internal reference. The longitudinal relaxation times (*T*1) of chalcone **3** protons and carbons were measured by the inversion recovery method, with a $(180^o\text{-}\tau\text{-}90^o)_n$ pulse sequence. For hydrogens, 16 recovery delays randomly ranged from 0.001 to 20 s were used for the solutions with and without BSA. For carbons, 44 recovery delays randomly ranged from 0.001 to 25 s were used for the solutions with and without BSA. Typically, NMR data were collected with 128 free induction decays (FIDs) and 64 K data points using a 6.7 μs pulse width (90º pulse angle) and an acquisition time of 3.27 s, using the same receiver gain. Prior to Fourier transformation, all FIDs were zero-filled and exponential weighing factor corresponding to a line broadening of 0.3 Hz were applied.

Theoretical calculations

Theoretical treatment of chalcone **3** was performed using the density functional theory (DFT) approach of the Gaussian 09 series of programs.(*1*) Geometry optimization of the ground (S_0) and first excited (S_1) states (in gas phase and water) were conducted with 6-311+g(2d,p) Pople's split-valence basis set and Becke's 3-parameter hybrid exchange-correlation functional (B3LYP).(*2, 3*) Harmonic frequency calculations were performed verify whether we have located a genuine minimum. The optimized geometries of S_0 and S_1 were used for the single point TD-DFT calculation using the Perdew-Burke-Erzenrhof exchange-correlation functional (PBE1PBE)(*4*) in combination with 6-311+G(2d,p). Absorption spectra in close agreement with experiments have been obtained using the TD-PBE1PBE/6-311+G(2d,p) level of calculation.(*5, 6*) To include the solvent effects in our quantum mechanics calculations we have employed the self-consistent reaction field (SCRF) approach with the polarizable continuum model (PCM)(*7-9*) were the solute molecule is enclosed in a cavity embedded in a dielectric medium.

The Fukui functions (*10*) were employed to determine the reactivity sites in chalcone **3**. The Fukui functions were employed to determine the reactivity sites in the molecule. This function, denoted as $f(\vec{r})$, is defined as the derivative of the electron density, $\rho(\vec{r})$, with respect to the total number of electrons of the system, N, under a constant external potential, $v(\vec{r})$:

$$f(\vec{r}) = \left[\frac{\partial \rho(\vec{r})}{\partial N}\right]_{v(\vec{r})} \quad (1)$$

Due to the discontinuity of the first derivative in Eq.(1) with respect to the number of electrons N, the following three functions can be defined in a finite difference approximation:

$$f^+(\vec{r}) = \rho(\vec{r})_{N+1} - \rho(\vec{r})_N \quad (2a)$$

$$f^-(\vec{r}) = \rho(\vec{r})_N - \rho(\vec{r})_{N-1} \quad (2b)$$

$$f^0(\vec{r}) = \frac{1}{2}[\rho(\vec{r})_{N+1} - \rho(\vec{r})_{N-1}] \quad (2c)$$

where $\rho(\vec{r})_{N+1}$, $\rho(\vec{r})_N$ and $\rho(\vec{r})_{N-1}$ are the electronic densities of the system with $N+1$, N, and $N-1$ electrons, respectively, all with the ground state geometry of the N electron system. Equations (2a), (2b), and (2c) are evaluated for nucleophilic, electrophilic and free radical attacks respectively. The finite difference formulation is frequently used in combination with the condensed Fukui function. The condensed Fukui functions can also be employed to determine the reactivity of each atom in the molecule. The corresponding condensed functions are given by

$$f_k^+ = q_k(N+1) - q_k(N) \quad \text{(for nucleophilic attack)} \quad (3a)$$

$$f_k^- = q_k(N) - q_k(N-1) \quad \text{(for electrophilic attack)} \quad (3b)$$

$$f_k^0 = [q_k(N+1) - q_k(N-1)]/2 \quad \text{(for radical attack)} \quad (3c)$$

where $q_k(N+1)$, $q_k(N)$ and $q_k(N-1)$ are the partial charges at atom k on the anion, neutral, and cations species, respectively. We calculated partial charges of each atom using CHELPG (Charges from Electrostatic Potentials using a Grid based) method.(*11*)

Atomic coordinates for BSA were taken from the crystallographic structure solved at 2.70 Å (PDB ID 3V03). Molecular docking simulations were performed with the program Autodock4[(12-14)] coupled to the AutoDock Tools.[(14, 15)] The partial charges on the protein and chalcone **3** atoms were taken from the AMBER all-atom force field.[(16)] The grid maps were calculated using AutoGrid.[(17)] Two different grid maps with 126 x 126 x 126 points and a grid-point spacing of 0.300 Å and 0.175 Å, respectively, were calculated. Each pair of grids was successively cantered on residues Trp134, Trp213 and Tyr410. During the docking simulations, dihedral angles were treated as flexible for chalcone **3** as well as for residues Glu17, Lys131, Lys 132, Arg198 and Arg217. The Lamarckian genetic algorithm was used with the following parameters:(*12-14*) an initial population of 100 random individuals, a maximum number of 1.5 x 10^6 energy evaluations, a maximum number of 27000 generations with mutation and crossover rates of 0.02 and 0.08, respectively. An optional elitism parameter equal to 1 was applied. It determines the number of top

individuals that will survive into the next generation. A maximum of 300 iterations per local search was allowed. The probability of performing a local search on an individual was 0.06 where the maximum number of consecutive successes or failures before doubling or halving the search step was 4. After the conformational search, the docked conformations were sorted in order of increasing energy. The coordinates of the lowest energy conformation were clustered based a root-mean-squared-deviation of 2.0 Å. A more detailed description of the methodology employed here can be found elsewhere.(*18, 19*)

Molecular dynamics simulations[20, 21] were carried out using the GROMOS force field force parameter set 53A6.[22, 23] The α-carbon atoms were position restrained with a force constant of 1000 kJ·mol^{-1}·nm^{-2} throughout the simulation. The system was placed in a cubic box of 8.0 x 8.0 x 8.0 nm^3, treated for periodic boundary conditions and solvated with explicit SPC model water molecules.[24] The system was neutralized with 16 Na^+ counter ions. Simulations were carried out in the NPT ensemble and a time step of 2 fs was used to integrate the equations of motion based on the Leap-Frog algorithm.[25] The temperature of the solute and solvent were separately coupled to the velocity rescale thermostat at 298.15 K with a relaxation time of 0.1 ps. The pressure was maintained as 1 atm by isotropic coordinate scaling with a relaxation time of 1 ps. Hydrogen bond lengths and angles were constrained by using the P-LINCS algorithm[26] and the geometry of the water molecules was constrained using the SETTLE algorithm.[27] A twin-range cutoff of 1.2 and 1.4 nm was used for vdW interactions. The pair-list for short-range non-bonded interactions was recomputed every 5 fs simultaneously with the update of the intermediate-range non-bonded interactions. The mean effect of electrostatic interactions beyond the long-range cutoff distance was approximated by the inclusion of a reaction-field force[28] using a solvent dielectric constant ε = 66. The systems were initially minimized through 20.000 iterations of the steepest descent algorithm. The system was simulated for 2.5 ns with configurations being recorded at every 5.0 ps. The software package GROMACS v.4.5.4 and implemented algorithms were used for simulation and analysis.[29] Protein structures were visualized with the software VMD 1.86.[30]

Circular Dichroism

Circular Dichroism (CD) measurements were carried out using Jasco J-815 spectropolarimeter (Jasco, Tokyo, Japan) equipped with a Peltier type temperature controller and thermostatized cuvette cell. Five consecutive measurements were accumulated and the averaged far and near UV spectra were recorded. The ellipticities were corrected for the baseline contribution of the buffer from each recorded spectrum and converted into molar ellipticity ([θ]) based on molecular mass per residue of 112 Da. Near-UV CD experiments were performed in order to estimate binding constant for BSA-chalcone **3** complex formation. Spectra were recorded from 250 to 475 nm upon varying amounts of chalcone (0 to 9.0 x 10^{-5} M) added to 3.0 x 10^{-5} M of BSA at 25 °C, in thermostatized quartz cuvettes of 1 cm pathway. The baseline of buffer and BSA spectra in the absence of **3** were subtracted from all spectra obtained from the titration experiment in order to collect the differential molar ellipticities as consequence of complex formation. The equilibrium of binding reaction was monitored from CD signal at 382 nm. Binding constant of the BSA-chalcone **3** complex, *Kd*, was calculated from fitted curve of $[\theta]_{382}$ nm as a function of chalcone concentration, according to Adair equation considering two binding sites, using the GRAFIT program version 3 (Erithacus Software, Horley, Surrey, United Kingdom). Far-UV spectra of BSA (3.0 x 10^{-7} M) and BSA in the presence of **3** (1.5 x 10^{-7} M) were recorded using 0.2 cm pathlength quartz cuvette in 5 mM tris-HCl buffer (pH 7.5). The BSA unfolding pathway induced by temperature increase was performed raising the temperature at 0.5 °C/min, from 25 °C to 95 °C. The BSA structure in the presence and absence of chalcone was monitored by changes in [θ] at 222 nm. The thermal denaturing curves were expressed considering the unfolded protein fraction (f_U) and the equilibrium constants (K_{eq}) were estimated according to equations 1 and 2. The thermodynamic parameters enthalpy (ΔH_m), entropy (ΔS_m) and the Gibbs free energy (ΔG^{25}) were calculated from van't Hoff approximation using equation 3 and equation 4.

$$f_U = (y_N - y) / (y_N - y_U) \quad (1)$$

$$K_{eq} = [U] / [N] = f_U / (1 - f_U) \quad (2)$$

$$R \ln K_{eq} = - \Delta H \, (1/T) + \Delta S \quad (3)$$

$$\Delta G = \Delta H - T \, \Delta S \quad (4)$$

In the equations, y_N and y_U represent the amount of *y* protein in native and unfolded states, respectively. [U] and [N] denote the protein concentration in unfolded and native states, respectively; *R*, the universal gas constant (1.987 cal·K^{-1}·mol^{-1}) and *T*, the temperature in Kelvin (K). The melting temperature (T_m), where the unfolding occurs, was calculated from the nonlinear fitting of unfolding curves.

Mass spectrometry

ESI-MS and ESI-MS/MS measurements were performed in the positive ion mode (m/z 50–2000 range) on a Waters Synapt HDMS (high definition mass spectrometer, Manchester, UK) instrument. This instrument has a hybrid

quadrupole/ion mobility/orthogonal acceleration time-of-flight (oa-TOF) geometry and was used in the TOF mode, with the mobility cell switched off and working only as an ion guide. All samples were dissolved in acetonitrile or methanol to form 50 μM solutions and were infused directly into the ESI source in a flow rate of 5 μL/min. ESI source conditions were as follows: capillary voltage 3.0 kV, sample cone 30 V, extraction cone 3 V. Native BSA/Chalcone ESI experimentswere performed by incubating BSA (100 μM) and chalcone structure (1 mM) in 50 mM ammonium acetate bufer (pH 7.0) for 4 hours at room temperature. The resulting sample was directly infused into mass spectrometer at 10 μl/min. Mass spectrometer parameters like cone voltage, source temperature, inner source pressure and cappilary voltave and distance to cone were scaned to verify the presence of BSA/Chalcone non-covalent adduct.

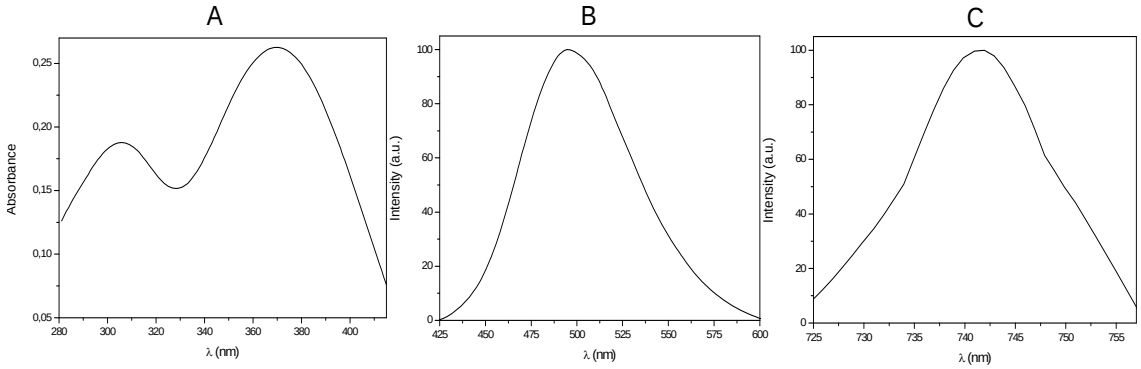

Figure S1. (A) UV-VIS of compound **3**. (B) Fluorescence emission at 494 nm. (C) Fluorescence emission at 742 nm. All experiments in methanol. Dye concentration = 10 μM.

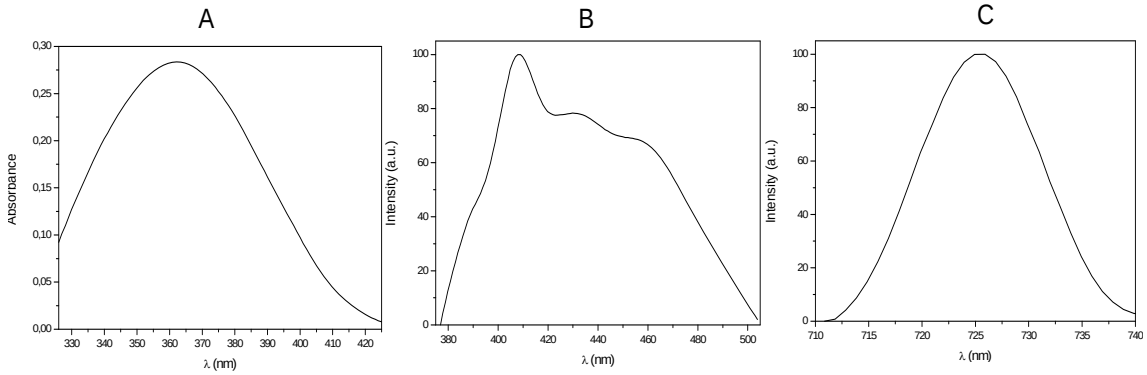

Figure S2. (A) UV-VIS of compound **3.** (B) Fluorescence emission at 408, 431 and 458 nm. (C) Fluorescence emission at 725 nm. All experiments in acetone. Dye concentration = 10 μM.

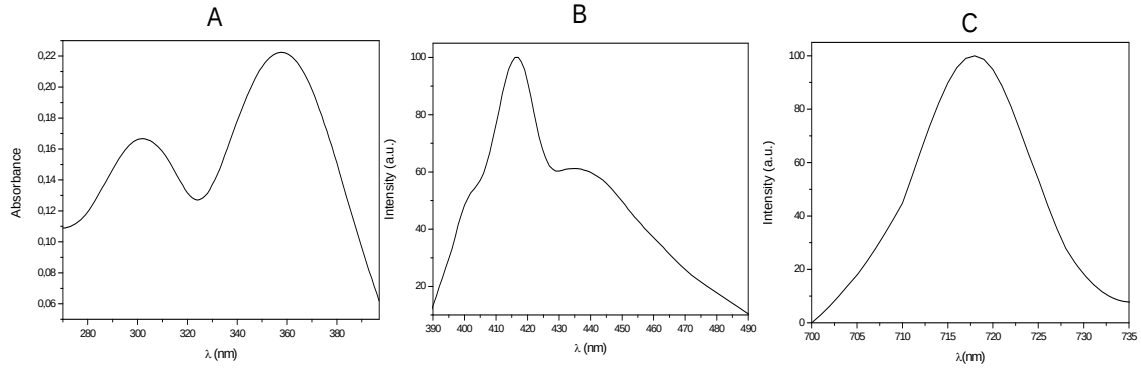

Figure S3. (A) UV-VIS of compound **3.** (B) Fluorescence emission at 416 and 437 nm. (C) Fluorescence emission at 718 nm. All experiments in 1,4-dioxane. Dye concentration = 10 μM.

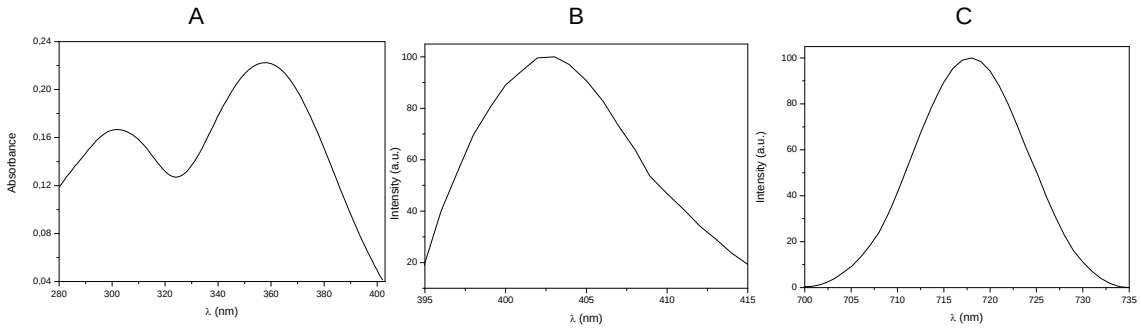

Figure S4. (A) UV-VIS of compound **3.** (B) Fluorescence emission at 403 nm. (C) Fluorescence emission at 718 nm. All experiments in ethyl acetate. Dye concentration = 10 μM.

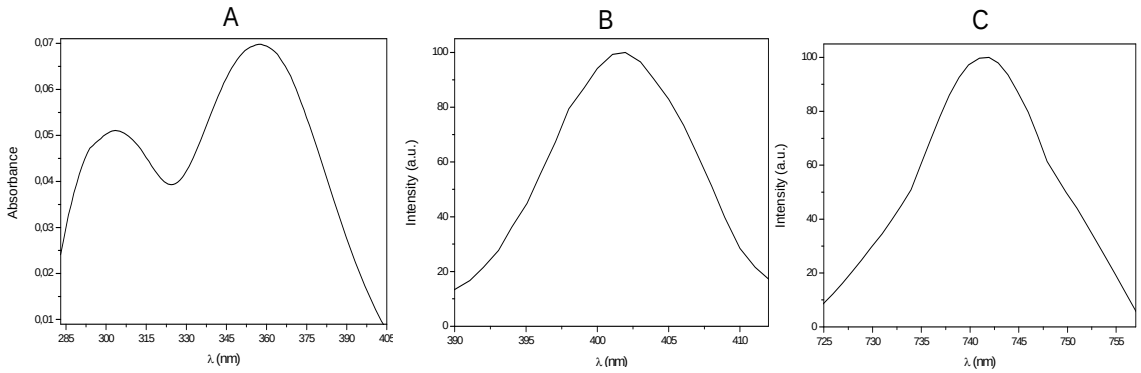

Figure S5. (A) UV-VIS of compound **3.** (B) Fluorescence emission at 402 nm. (C) Fluorescence emission at 716 nm. All experiments in toluene. Dye concentration = 10 μM.

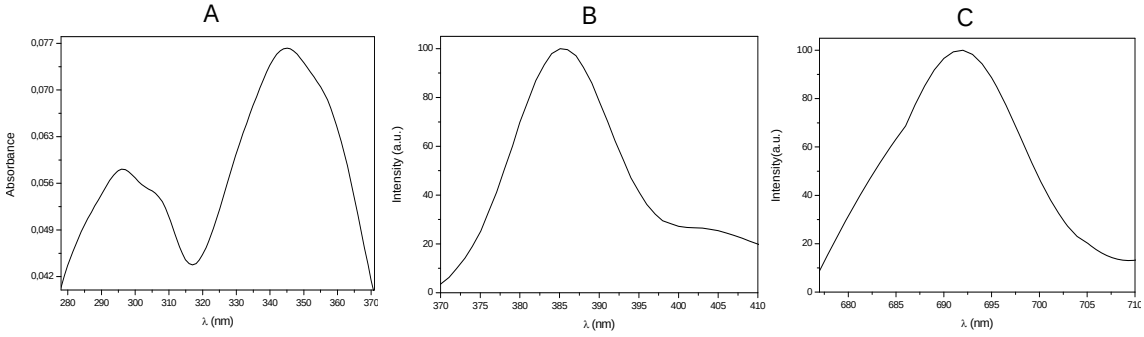

Figure S6. (A) UV-VIS of compound **3.** (B) Fluorescence emission at 385nm. (C) Fluorescence emission at 692 nm. All experiments in hexane. Dye concentration = 10 μM.

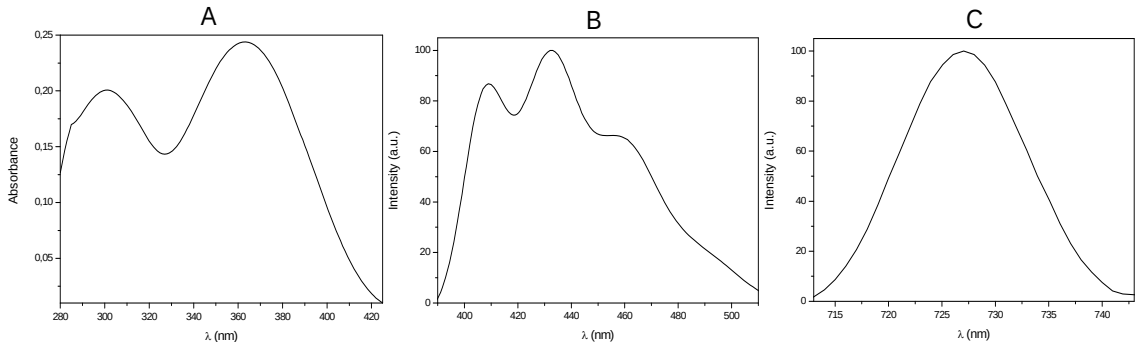

Figure S7. (A) UV-VIS of compound **3.** (B) Fluorescence emission at 409, 433 and 458 nm. (C) Fluorescence emission at 727 nm. All experiments in dichloromethane. Dye concentration = 10 μM.

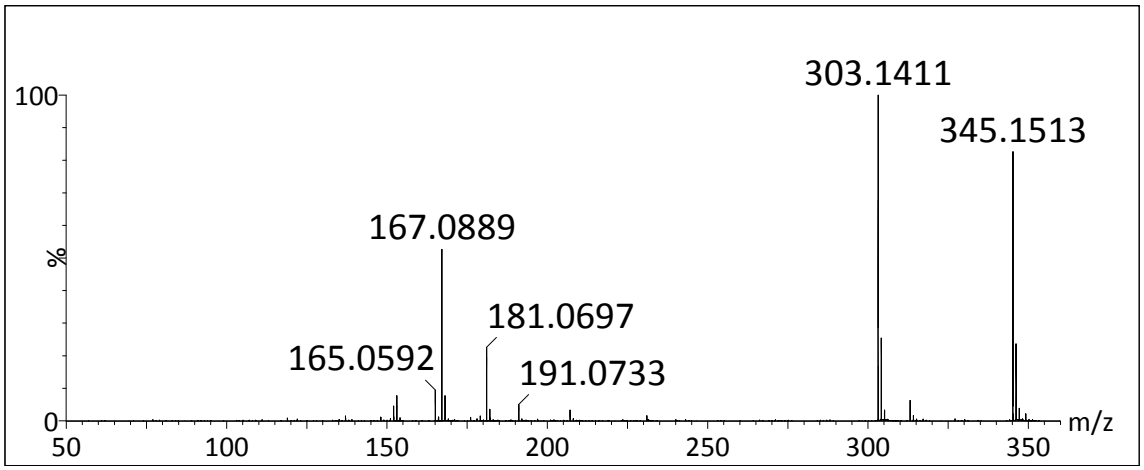

Figure S8. ESI(+)-QTOF-MS/MS (collision induced dissociation) of protonated chalcone derivative **3**. Precursor ion of *m/z* 345.15.

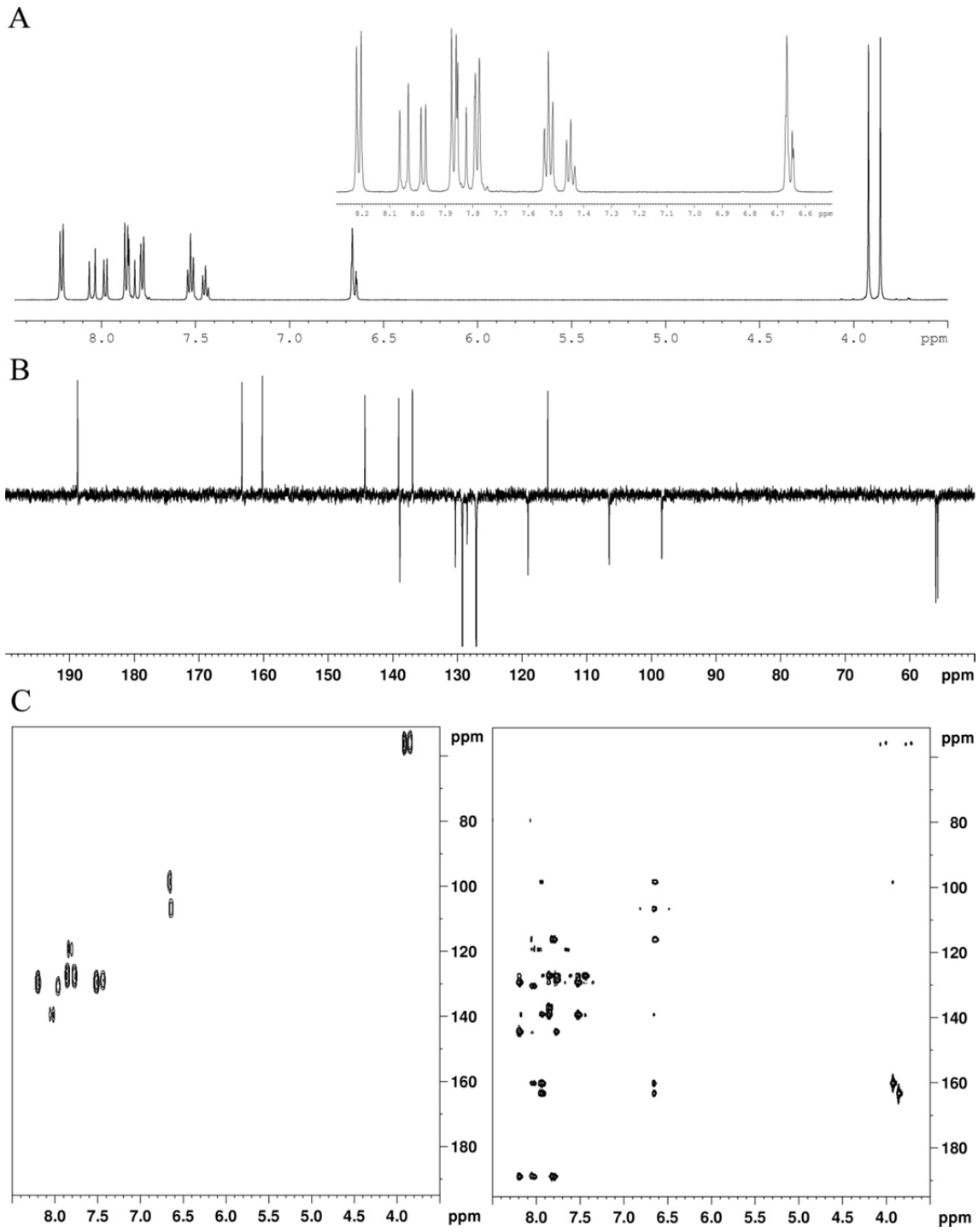

Figure S9. (**A**) ^{1}H, (**B**) ^{13}C APT and (**C**) ^{1}H-^{13}C HSQC (left) and HMBC (right) spectra. Dye concentration = 200 mM (DMSO-*d6*).

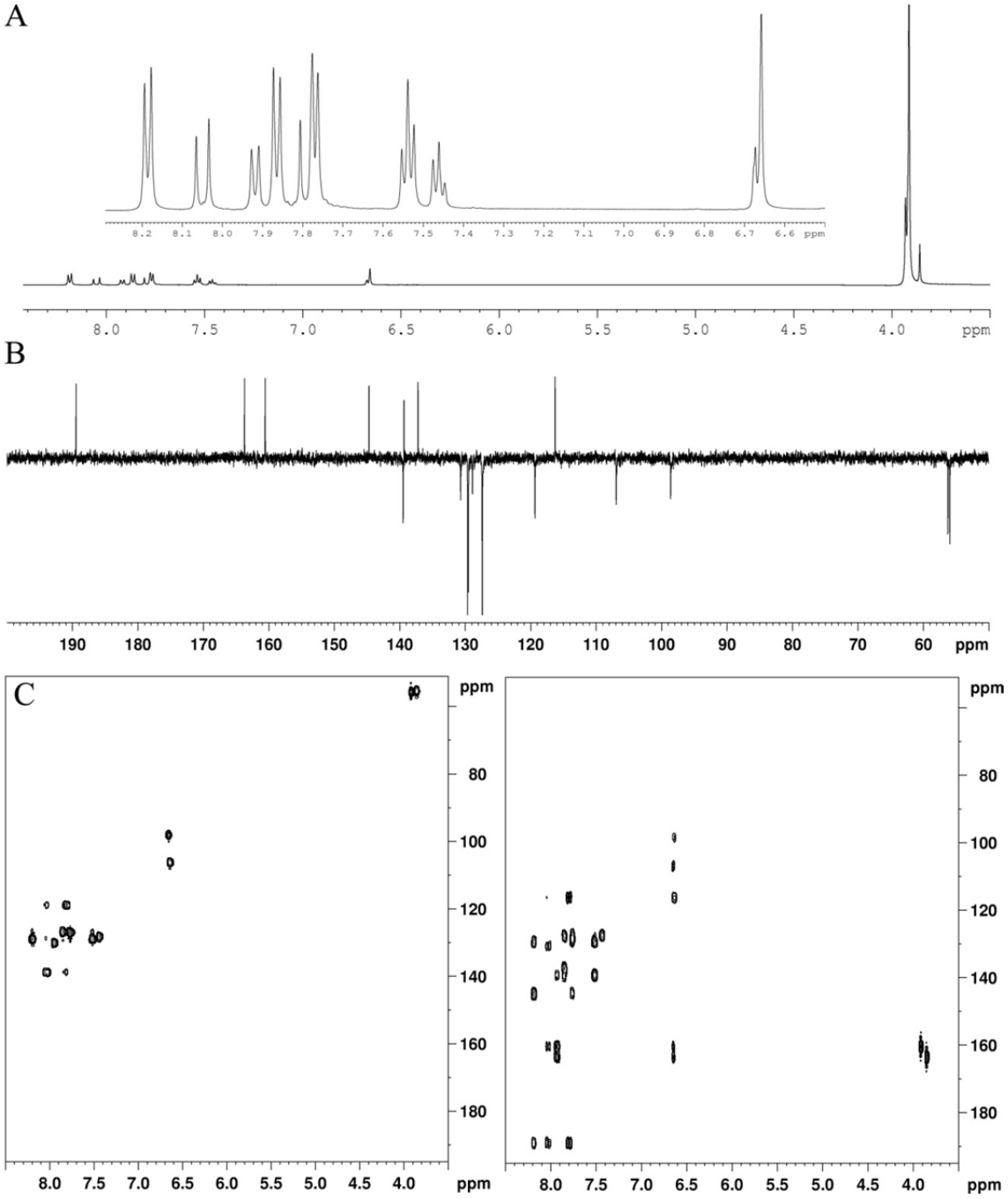

Figure S10. (**A**) ^{1}H, (**B**) ^{13}C APT and (**C**) ^{1}H-^{13}C HSQC (left) and HMBC (right) with BSA final concentration of 15 μM (from D_2O solution). Dye concentration = 200 mM (DMSO-*d6*).

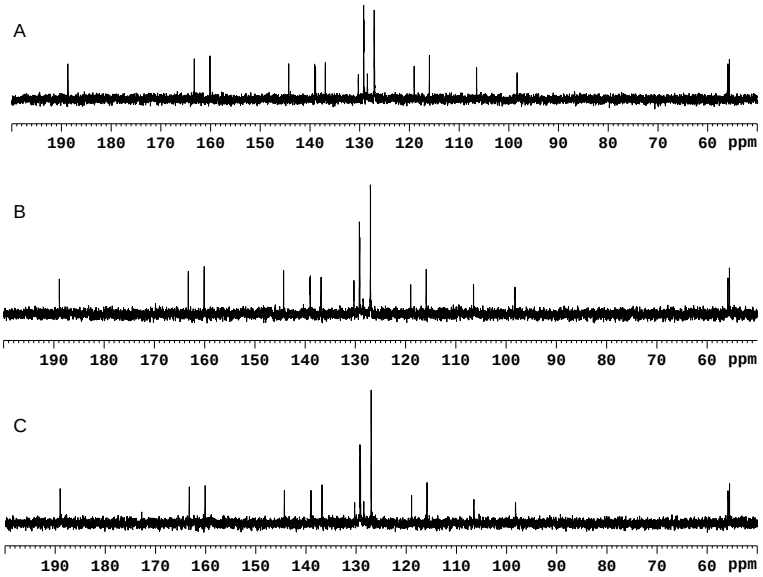

Figure S11. ^{13}C NMR spectra of (A) 200 mM solution of **3** in DMSO-*d6* , (B) with 10 μM and (C) with 15 μM of BSA.

Table S1. ^{1}H T1(s) of a 200 mM of chalcone **3** and 2.5 μM, 10.0 μM and 15.0 μM of BSA (host), respectively.

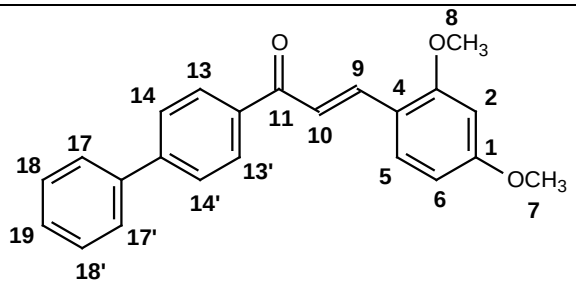

Structure of **3**

Position	Guest (chalcone 3)	3 + BSA (2.5 μM)	3 + BSA (10 μM)	3 + BSA (15 μM)
1	-	-	-	-
2	1.31	1.39	*	*
3	-	-	-	-
4	-	-	-	-
5	1.05	1.12	1.34	1.24
6	1.50	1.39	*	*
7	0.67	0.77	0.64	*
8	0.64	0.75	0.77	*
9	2.66	2.93	2.72	2.49
10	0.92	1.16	1.24	1.07
11	-	-	-	-
12	-	-	-	-
13 e 13’	1.44	1.49	1.66	1.67
14 e 14’	1.23	1.61	1.64	1.55
15	-	-	-	-
16	-	-	-	-
17 e 17’	1.48	1.47	1.56	1.44
18 e 18’	1.71	1.77	1.96	1.66
19	1.91	1.95	1.97	1.93

* T1 values were not calculated due to signal superposition.

Table S2. Fukui function (f^+ and f^- values) for all carbon atoms of the fluorescent chalcone **3**. Values in brackets were obtained considering the solvent effect (simulated in water).

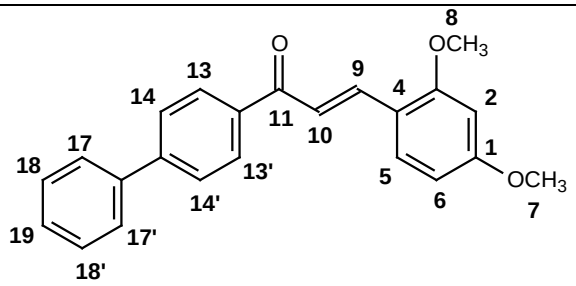

Structure of **3**

Atom	State (ground or first excited)	Fukui function values (f^+)	Fukui function values (f^-)
C1	S_0	0.03 [0.03]	0.05 [0.05]
C1	S_1	0.05 [0.02]	0.05 [0.06]
C2	S_0	0.01 [0.01]	-0.01 [0.01]
C2	S_1	0.01 [0.01]	-0.01 [0.00]
C3	S_0	0.02 [0.02]	0.03 [0.02]
C3	S_1	0.03 [0.02]	0.03 [0.02]
C4	S_0	-0.02 [0.00]	0.13 [0.22]
C4	S_1	-0.03 [-0.01]	0.10 [0.23]
C5	S_0	0.02 [0.03]	-0.04 [-0.06]
C5	S_1	0.03 [0.03]	-0.03 [-0.07]
C6	S_0	0.04 [0.04]	0.10 [0.16]
C6	S_1	0.04 [0.06]	0.07 [0.15]
C7	S_0	-0.05 [-0.04]	-0.05 [-0.05]
C7	S_1	-0.06 [-0.06]	-0.05 [-0.03]
C8	S_0	-0.06 [-0.05]	-0.02 [-0.03]
C8	S_1	-0.07 [-0.06]	-0.02 [-0.02]
C9	S_0	0.11 [0.13]	-0.05 [-0.08]
C9	S_1	0.14 [0.09]	-0.04 [-0.06]
C10	S_0	-0.01 [0.03]	0.21 [0.27]
C10	S_1	0.00 [0.05]	0.20 [0.24]
C11	S_0	0.13 [0.15]	-0.06 [-0.03]
C11	S_1	0.11 [0.12]	-0.07 [0.01]
C12	S_0	-0.04 [-0.02]	0.02 [-0.02]
C12	S_1	-0.04 [-0.01]	0.03 [-0.05]
C13	S_0	0.00 [0.01]	0.01 [0.03]
C13	S_1	-0.01 [0.00]	0.01 [0.03]
C13’	S_0	0.04 [0.05]	-0.01 [0.01]
C13’	S_1	0.02 [0.05]	0.00 [0.02]
C14	S_0	0.04 [0.04]	0.02 [0.00]
C14	S_1	0.03 [0.03]	0.01 [0.01]
C14’	S_0	0.01 [0.01]	0.02 [0.00]
C14’	S_1	0.01 [-0.02]	0.01 [0.03]
C15	S_0	0.06 [0.04]	0.04 [0.02]
C15	S_1	0.05 [0.08]	0.05 [-0.02]
C16	S_0	-0.02 [0.00]	-0.01 [-0.01]
C16	S_1	-0.03 [-0.04]	-0.01 [0.02]
C17	S_0	0.01 [0.00]	0.02 [0.01]
C17	S_1	0.01 [0.02]	0.02 [-0.01]
C17’	S_0	0.00 [0.00]	0.020 [0.01]
C17’	S_1	0.00 [0.00]	0.02 [0.01]
C18	S_0	0.01 [0.01]	0.01 [0.00]
C18	S_1	0.01 [0.02]	0.01 [-0.01]
C18’	S_0	0.02 [0.00]	0.00 [0.00]
C18’	S_1	0.01 [0.01]	0.00 [0.01]
C19	S_0	0.03 [0.02]	0.07 [0.01]
C19	S_1	0.03 [0.02]	0.07 [0.01]

References

1. Frisch, M. J., Trucks, G. W., Schlegel, H. B., Scuseria, G. E., Robb, M. A., Cheeseman, J. R., Scalmani, G., Barone, V., Mennucci, B., Petersson, G. A., Nakatsuji, H., Caricato, M., Li, X., Hratchian, H. P., Izmaylov, A. F., Bloino, J., Zheng, G., Sonnenberg, J. L., Hada, M., Ehara, M., Toyota, K., Fukuda, R., Hasegawa, J., Ishida, M., Nakajima, T., Honda, Y., Kitao, O., Nakai, H., Vreven, T., Montgomery, J. A., Peralta, J. E., Ogliaro, F., Bearpark, M., Heyd, J. J., Brothers, E., Kudin, K. N., Staroverov, V. N., Kobayashi, R., Normand, J., Raghavachari, K., Rendell, A., Burant, J. C., Iyengar, S. S., Tomasi, J., Cossi, M., Rega, N., Millam, J. M., Klene, M., Knox, J. E., Cross, J. B., Bakken, V., Adamo, C., Jaramillo, J., Gomperts, R., Stratmann, R. E., Yazyev, O., Austin, A. J., Cammi, R., Pomelli, C., Ochterski, J. W., Martin, R. L., Morokuma, K., Zakrzewski, V. G., Voth, G. A., Salvador, P., Dannenberg, J. J., Dapprich, S., Daniels, A. D., Farkas, Foresman, J. B., Ortiz, J. V., Cioslowski, J., and Fox, D. J. (2009) Gaussian 09, Revision A.02, Wallingford CT.
2. Becke, A. D. (1993) Density-functional thermochemistry .3. the role of exact exchange, *J. Chem. Phys. 98*, 5648-5652.
3. Lee, C. T., Yang, W. T., and Parr, R. G. (1988) Development Of The Colle-Salvetti Correlation-Energy Formula Into A Functional Of The Electron-Density, *Phys. Rev. B 37*, 785-789.
4. Perdew, J. P., Burke, K., and Ernzerhof, M. (1996) Generalized gradient approximation made simple, *Phys. Rev. Lett. 77*, 3865-3868.
5. Fonseca, T. L., de Oliveira, H. C. B., and Castro, M. A. (2008) Theoretical study of the lowest electronic transitions of sulfur-bearing mesoionic compounds in gas-phase and in dimethyl sulfoxide, *Chem. Phys. Lett. 457*, 119-123.
6. Marana, N. L., Longo, V. M., Longo, E., Martins, J. B. L., and Sambrano, J. R. (2008) Electronic and structural properties of the (10(1)over-bar0) and (11(2)over-bar0) ZnO surfaces, *J. Phys. Chem. A 112*, 8958-8963.
7. Miertus, S., Scrocco, E., and Tomasi, J. (1981) Electrostatic interaction of a solute with a continuum - a direct utilization of abinitio molecular potentials for the prevision of solvent effects, *Chem. Phys. 55*, 117-129.
8. Cammi, R., and Tomasi, J. (1995) Remarks on the use of the apparent surface-charges (asc) methods in solvation problems - iterative versus matrix-inversion procedures and the renormalization of the apparent charges, *J. Comput. Chem. 16*, 1449-1458.
9. Tomasi, J., Mennucci, B., and Cammi, R. (2005) Quantum mechanical continuum solvation models, *Chem Rev 105*, 2999-3093.
10. Parr, R. G., and Yang, W. T. (1984) Density functional-approach to the frontier-electron theory of chemical-reactivity, *J. Am. Chem. Soc. 106*, 4049-4050.
11. Breneman, C. M., and Wiberg, K. B. (1990) Determining atom-centered monopoles from molecular electrostatic potentials - the need for high sampling density in formamide conformational-analysis, *J. Comput. Chem. 11*, 361-373.
12. Morris, G. M., Goodsell, D. S., Halliday, R. S., Huey, R., Hart, W. E., Belew, R. K., and Olson, A. J. (1998) Automated docking using a Lamarckian genetic algorithm and an empirical binding free energy function, *J Comput Chem 19*, 1639-1662.
13. Huey, R., Morris, G. M., Olson, A. J., and Goodsell, D. S. (2007) A semiempirical free energy force field with charge-based desolvation, *J Comput Chem 28*, 1145-1152.
14. Morris, G. M., Huey, R., Lindstrom, W., Sanner, M. F., Belew, R. K., Goodsell, D. S., and Olson, A. J. (2009) AutoDock4 and AutoDockTools4: Automated docking with selective receptor flexibility, *J Comput Chem 30*, 2785-2791.
15. Sanner, M. F. (1999) Python: a programming language for software integration and development, *J Mol Graph Model 17*, 57-61.
16. Weiner, S. J., Kollman, P. A., Nguyen, D. T., and Case, D. A. (1986) An all atom force field for simulations of proteins and nucleic acids, *J Comput Chem 7*, 230-252.

17. Goodford, P. J. (1985) A computational procedure for determining energetically favorable binding sites on biologically important macromolecules, *J. Med. Chem. 28*, 849-857.
18. Soares, T. A., Goodsell, D. S., Briggs, J. M., Ferreira, R., and Olson, A. J. (1999) Docking of 4-oxalocrotonate tautomerase substrates: implications for the catalytic mechanism, *Biopolymers 50*, 319-328.
19. Soares, T. A., Lins, R. D., Straatsma, T. P., and Briggs, J. M. (2002) Internal dynamics and ionization states of the macrophage migration inhibitory factor: comparison between wild-type and mutant forms, *Biopolymers 65*, 313-323.
20. van Gunsteren, W. F., Bakowies, D., Baron, R., Chandrasekhar, I., Christen, M., Daura, X., Gee, P., Geerke, D. P., Glattli, A., Hunenberger, P. H., Kastenholz, M. A., Ostenbrink, C., Schenk, M., Trzesniak, D., and van der Vegt, N. F. A. (2006) Biomolecular modeling: Goals, problems, perspectives, *Angew Chem Int Edit 45*, 4064-4092.
21. Soares, T. A., Hunenberger, P. H., Kastenholz, M. A., Krautler, V., Lenz, T., Lins, R. D., Oostenbrink, C., and van Gunsteren, W. F. (2005) An improved nucleic acid parameter set for the GROMOS force field, *J. Comput. Chem. 26*, 725-737.
22. Oostenbrink, C., Soares, T. A., van der Vegt, N. F. A., and van Gunsteren, W. F. (2005) Validation of the 53A6 GROMOS force field, *Eur Biophys J Biophy 34*, 273-284.
23. Soares, T. A., Daura, X., Oostenbrink, C., Smith, L. J., and van Gunsteren, W. F. (2004) Validation of the GROMOS force-field parameter set 45A3 against nuclear magnetic resonance data of hen egg lysozyme, *J Biomol Nmr 30*, 407-422.
24. Berendsen, H. J. C., Postma, J. P. M., van Gunsteren, W. F., and J., H. (1981) Interaction models for water in relation to protein hydration, In *Intermolecular Forces* (Pullman, B., Ed.), pp 331-342, Reidel, Dordrecht.
25. van Gunsteren, W. F., and Berendsen, H. J. C. (1988) A leap-frog algorithm for stochastic dynamics, *Molecular Simulation 1*, 173-185.
26. Hess, B., Bekker, H., Berendsen, H. J. C., and Fraaije, J. G. E. M. (1997) LINCS: A linear constraint solver for molecular simulations, *J. Comput. Chem. 18*, 1463-1472.
27. Miyamoto, S., and Kollman, P. A. (1992) Settle - an Analytical Version of the Shake and Rattle Algorithm for Rigid Water Models, *J. Comput. Chem. 13*, 952-962.
28. Tironi, I. G., Sperb, R., Smith, P. E., and van Gunsteren, W. F. (1995) A generalized reaction field method for molecular dynamics simulations, *J Chem Phys 102*, 5451-5459.
29. Hess, B., Kutzner, C., van der Spoel, D., and Lindahl, E. (2008) GROMACS 4: Algorithms for highly efficient, load-balanced, and scalable molecular simulation, *Journal of Chemical Theory and Computation 4*, 435-447.
30. Humphrey, W., Dalke, A., and Schulten, K. (1996) VMD: Visual molecular dynamics, *J Mol Graphics 14*, 33.